Geochemical Perspectives Letters

Accessory mineral constraints on crustal evolution: elemental fingerprints for magma discrimination

E. Bruand[1]*, M. Fowler[2], C. Storey[2], O. Laurent[3], C. Antoine[1], M. Guitreau[1], E. Heilimo[4], O. Nebel[5]

OPEN ACCESS

doi: 10.7185/geochemlet.2006

Abstract

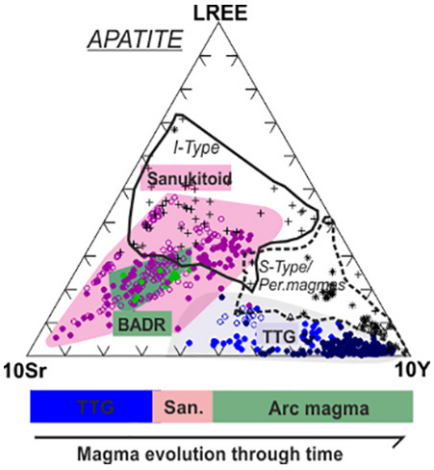

Underexplored accessory minerals such as titanite and apatite have the potential to give insights into the nature and the petrogenesis of their host rock. Their trace element and REE-rich compositions carry a record of crystallisation history and chemical characteristics of their source. Moreover, titanite and, to a certain extent, apatite are resistant to erosion during sedimentary cycles which makes them ideal to reconstruct the history of long-eroded continental landmasses. Here we report new trace element data on apatite and titanite from granitoids of different Archean cratons and comparative granitoids from the Phanerozoic. Trace element signatures of both minerals reveal systematic chemical trends in Y, LREE and Sr contents related to the nature of their host magma, which are used to construct discrimination diagrams delineating Archean TTGs from sanukitoids, and modern adakites from S/I-type granites. By comparing Archean granitoids (TTG and sanukitoids) and their Phanerozoic counterparts (adakite and high Ba-Sr granites), we show that the robust nature of these phases makes them reliable recorders of petrogenetic information from Archean rocks, that usually have been affected by secondary processes (metamorphism, deformation, hydrothermal activity). Applied to the rock record, both phases potentially provide detailed archives of magmatic evolution through time.

Received 27 August 2019 | Accepted 18 January 2020 | Published 26 February 2020

Introduction

Rare earth element (REE) bearing minerals have been used widely to date geological events and are prime archives for magmatic petrogenesis. Their ability to incorporate a range of trace elements in addition to REE make them extremely useful to track geological processes. While most studies on accessory minerals have focussed on zircon (*e.g.*, U-Pb, Hf isotopes, O isotopes, trace elements), the development of more advanced *in situ* techniques has also facilitated other phases to be dated (*e.g.*, monazite, Kohn and Vervoort, 2008; titanite, Storey *et al.*, 2007), thus providing additional chronological constraints on host rock history. However, despite the impressive number of studies on accessory minerals available today (see Nasdala *et al.*, 2017), knowledge of the behaviour of trace elements within accessory minerals in rocks that make up the continental crust is still limited. The few contributions focussing on less-studied, REE-bearing minerals (*e.g.*, apatite and titanite, Belousova *et al.*, 2001; Chu *et al.*, 2009; Bruand *et al.*, 2014) have shown that trace element concentrations retain considerable information relevant to petrogenesis and provenance, potentially even more than zircon, whose compositional variability in the most common continental igneous rocks (*e.g.*, granitoids, Grimes *et al.*, 2015) is relatively limited. In experimental work focussing on metaluminous compositions, Protwake and Klemme (2005, 2006) have suggested that REE and other trace elements are sensitive to melt evolution. Recent publications based on a small number of samples (Bruand *et al.*, 2016, 2017, 2019) have shown that apatite and titanite trace element chemistry combined with O isotopes are useful tracers of granitoid petrogenesis and therefore have the potential to discriminate the different magmas through time and could provide an opportunity to track the secular evolution of the early Earth and the onset of modern style plate tectonics. For this contribution, we have studied the chemical signatures of accessory minerals in a range of crust-forming granitoids through time, from a relatively hot Archean Earth producing "tonalites-trondjhemites-granodiorites" (TTG)

1. Laboratoire Magmas et Volcans, Campus Universitaire des Cezeaux, 6 avenue Blaise Pascal, 63718 Aubiere, France
2. School of Earth and Environmental Sciences, University of Portsmouth, PO1 3QL, United Kingdom
3. Geosciences Environnement Toulouse, Université de Toulouse, 31400 Toulouse, France
4. Geotalo, Akatemiankatu 1, University of Turku, Finland
5. School of Earth, Atmosphere and Environment, Monash University, Melbourne, Australia

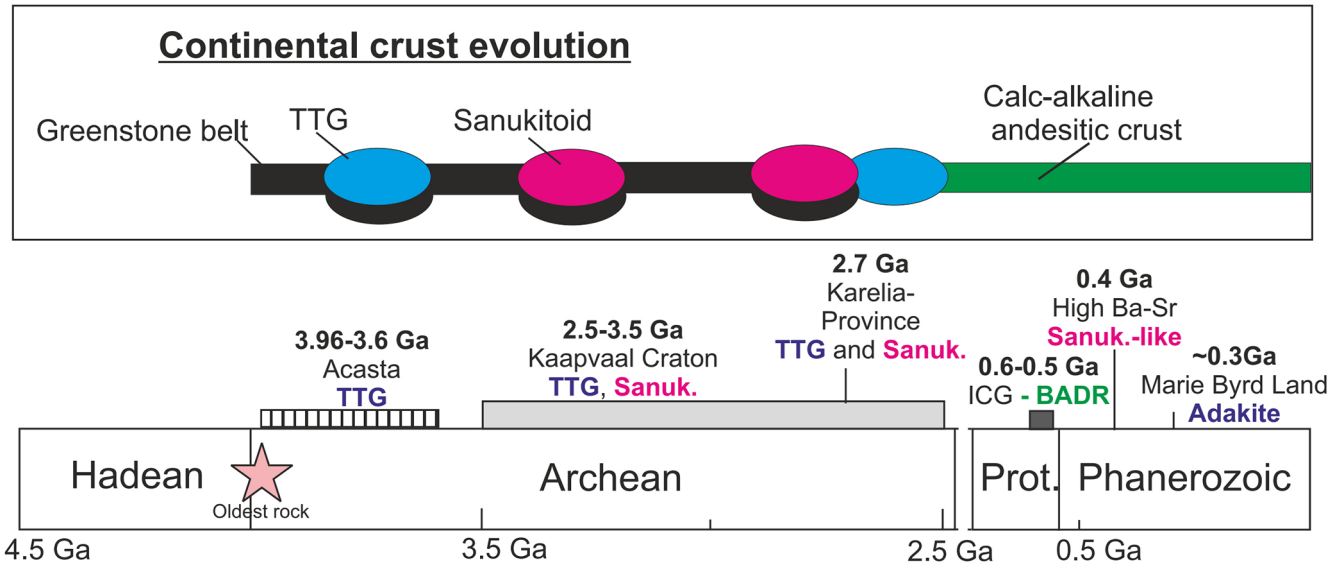

Figure 1 Cartoon of continental crust evolution, from TTG (blue) and sanukitoid (pink) in the Archean towards typical arc magma (green) in Proterozoic and Phanerozoic, plus samples studied in this contribution.

toward a cooler modern Earth producing plutonic equivalents of the calc-alkaline series (basalt-andesite-dacite-rhyolite, or BADR), *via* the Neoarchean – Palaeoproterozoic transition to modern plate tectonics signalled by sanukitoids and related rocks. We demonstrate that their trace element signatures can be used to discriminate between critical magma types and can be robust with respect to metamorphism. We then discuss the causes of consistent differences in accessory mineral chemistry and implications of their robust discrimination for studies of magmatic and crustal evolution through geological times.

Granitoid Samples and their Crustal Evolution Context

The granitoid record (Fig. 1) has evolved from the Archean to the Phanerozoic, as a reflection of Earth's cooling and evolution of tectono-magmatic processes (see Moyen and Laurent, 2018 and references therein). Granitoids representing newly formed continental crust have hence changed from Archean TTGs, formed by partial melting of mafic crust, *via* sanukitoids and related rocks in the Neoarchean and Palaeoproterozoic that carry the signature of a nascent mantle wedge, towards granodiorites and granites with arc magma compositions (the plutonic equivalents of BADR). Many fundamental questions remain regarding the geodynamics of the early Earth, the growth of the continental crust and the transition to subduction-driven tectonics, some of which may be addressed with a more complete understanding of timings and proportions of granitoid magma genesis. Here we present new geochemical data on titanite and apatite from granitoids selected from this overall temporal progression; (i) Archean TTG from three different cratons (Slave Province, Karelia and Kaapvaal), (ii) sanukitoids from the Karelia and Kaapvaal cratons, (iii) Neoproterozoic calc-alkaline granitoids from Guernsey (UK Channel Islands) in the Armorican terrane. Studied Archean localities have been affected by metamorphic conditions up to amphibolite facies. In addition to these, we have included likely Phanerozoic equivalents to test the impact of metamorphism on their older counterparts: TTG-like (adakites from Antarctica; Pankhurst *et al.*, 1998) and sanukitoid-like rocks (high Ba-Sr granites from Caledonian Scotland; Fowler and Rollinson, 2012). Detailed sample descriptions, geological settings and whole rock compositions can be found in the Supplementary Information.

Results

Trace element concentrations obtained by LA-ICPMS on single minerals and related analytical protocols are described in the Supplementary Information. After initial data interrogation using principal component analysis (PCA) on both apatite and titanite datasets, REEs, Y and Sr were found to be most effective for discriminating magma type. These results are presented and discussed below.

Apatite chemistry. Chondrite normalised REE patterns for apatite from all studied samples are plotted on Figure 2a-e. TTG samples (Fig. 2a) are characterised by a systematic depletion in light REE (LREE) relative to heavy REE (HREE; $La_N/Lu_N < 1$) usually with a strong negative Eu anomaly (usually Eu/Eu* = 0.15-0.8). The most depleted patterns tend to have a less pronounced to absent Eu anomaly and noticeable middle REE (MREE) fractionation from HREE. Adakite (TTG-like) apatite crystals (Fig. 2b) have a relatively flat LREE pattern (La_N/Sm_N = 0.5-1.8) with slightly lower HREE (La_N/Lu_N = 1.5-4) and a negative Eu anomaly (Eu/Eu* = 0.3-0.4). Typical BADR REE patterns (Fig. 2c) show higher LREE content with strong enrichment compared to the HREE ($La_N/Lu_N > 15$), with moderate negative Eu anomalies (Eu/Eu* ≈ 0.5). Similarly, sanukitoids and high Ba-Sr granite REE patterns (Fig. 2d,e) reveal a general enrichment in LREE relative to HREE (La_N/Lu_N = 10-100) usually with moderate negative Eu anomalies (Eu/Eu* ≈ 0.4-0.8). In the high Ba-Sr group, the most mafic samples often lack Eu anomalies.

Following the PCA procedure, a 10*Sr-LREE-10*Y discrimination diagram was constructed (Fig. 3a). Apatite from TTG and TTG-like granitoids are clearly distinguishable from other granitoid types, defining a distinct cluster towards the 10*Y corner and having Sr contents ranging between 150 and 430 µg/g (Table S-3). On the other hand, sanukitoids, sanukitoid-like and BADR samples are characterised by higher LREE and Sr contents (up to 1000 µg/g) and thus form a separate field towards that baseline. Similarly, a La_N/Sm_N *versus* Y diagram (Fig. 4a) highlights a strong compositional difference. TTG and TTG-like apatite grains are Y-rich (up to

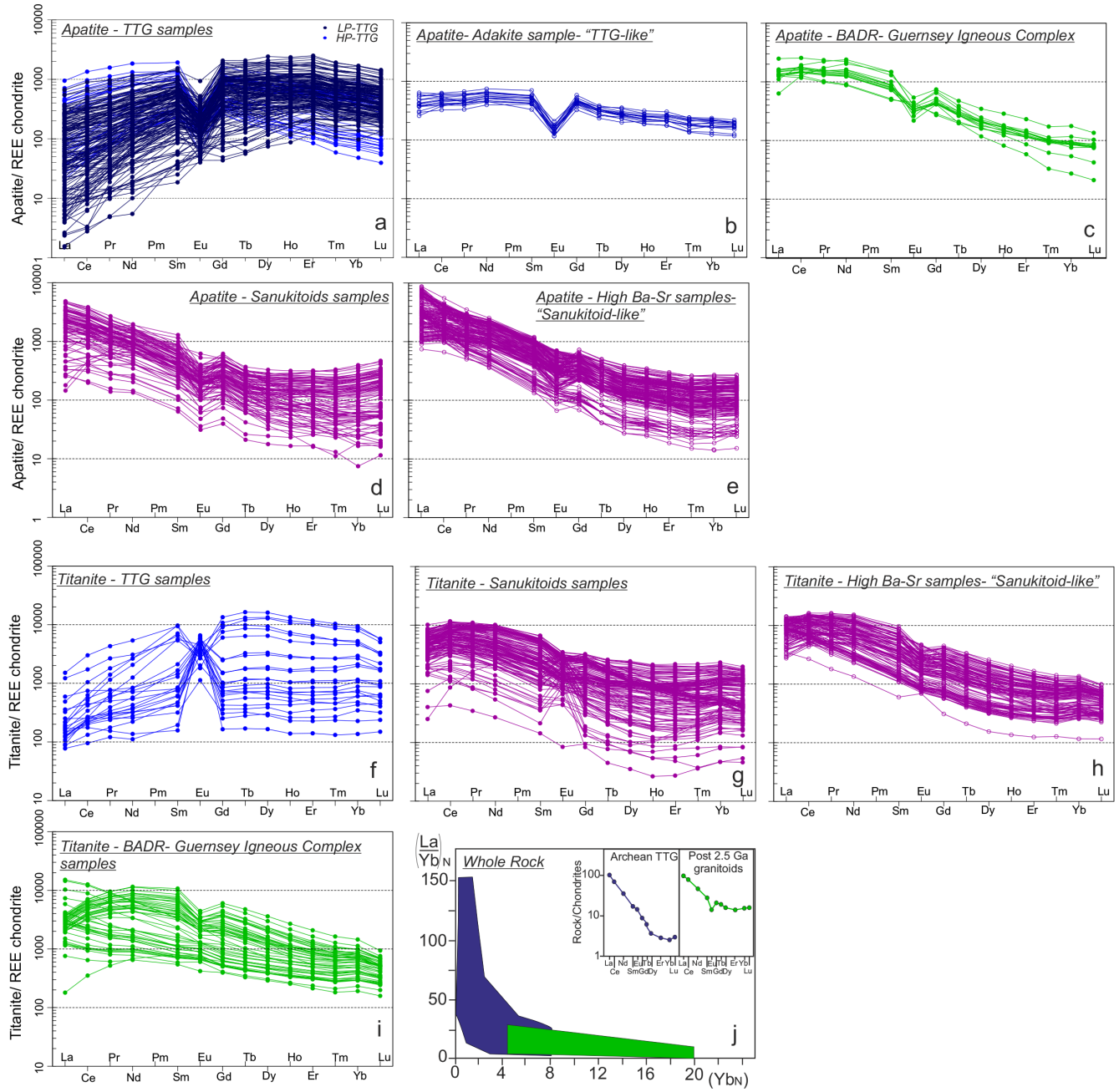

Figure 2 Chondrite normalised REE patterns for apatite **(a-e)** and titanite **(f-i)**. Diagram **j** represents La/Yb *vs.* Yb values normalised to chondrite for whole rock data, modified after Moyen and Martin (2012). Green and blue fields correspond to post 2.5 Ga granitoids and TTG, respectively.

approximately 4600 µg/g) with low La (<300 µg/g), whereas sanukitoid, high Ba-Sr granite and BADR apatite grains define a field poor in Y (<1000 µg/g) and with La up to approximately 2800 µg/g.

Titanite chemistry. REE patterns of titanite from the studied samples are presented in Figure 2f-i, although titanite is not present in all studied samples (see Supplementary Information). There are many similarities with the patterns for apatite (Fig. 2a-e). Titanite grains from one TTG sample (Fig. 2f) are characterised by pronounced LREE depletion relative to HREE (usually $La_N/Lu_N < 0.5$). In contrast with apatite, the patterns have variable, usually large Eu anomalies (Eu/Eu* = 0.2-40), generally negative for those with higher total REE, positive for lower total REE. Titanite from sanukitoids and high Ba-Sr granites (Fig. 2g,h) show strong enrichment of LREE relative to HREE ($La_N/Lu_N \approx 3$-45), usually with a convex upward LREE section and a noticeable negative Eu anomaly. A few sanukitoid titanites in each of the samples studied have steep downward LREE slopes and/or a positive Eu anomaly (Fig. 2g). The BADR REE patterns (Fig. 2i) are closely comparable with the high Ba-Sr samples, but can be separated into two groups that are sample specific. Sample EG-07 titanite crystals have convex upward LREE (La_N/Sm_N = 0.4-0.9) and a negative Eu anomaly (Eu/Eu* ≈ 0.6-0.7) whereas one from sample BD-02 has continually decreasing LREE ($La_N/Sm_N > 1$) with no Eu anomaly (Fig. 2i, Table S-3 in Supplementary Information).

Using a similar trivariate diagram to apatite (Fig. 3b, but note the different Sr multiplier accounting for lower Sr contents in titanite), TTG titanite compositions may be discriminated from all other samples. Titanite from TTG define an end member with high Y (up to 24000 µg/g) and low Sr (usually <20 µg/g) and LREE (*e.g.*, usually La < 150 µg/g) contents relative to sanukitoids and BADR samples (Y and La contents are up to 4000 µg/g; Sr > 40 µg/g).

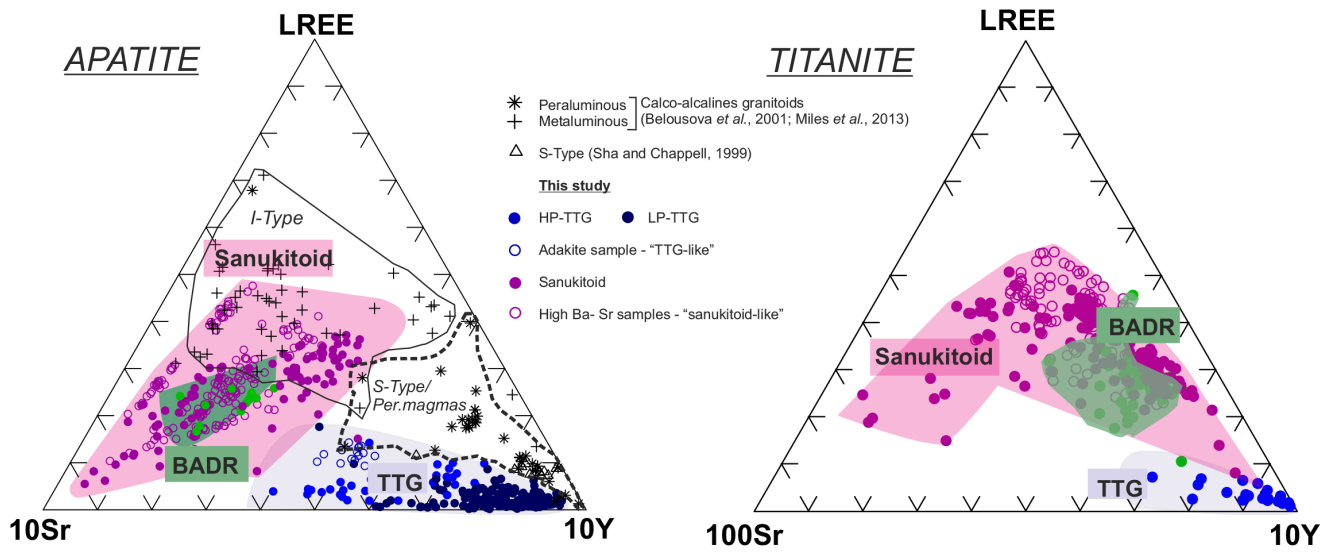

Figure 3 Ternary discrimination diagrams; 10*Sr-LREE-10*Y for apatite and 100*Sr-LREE-10*Y for titanite.

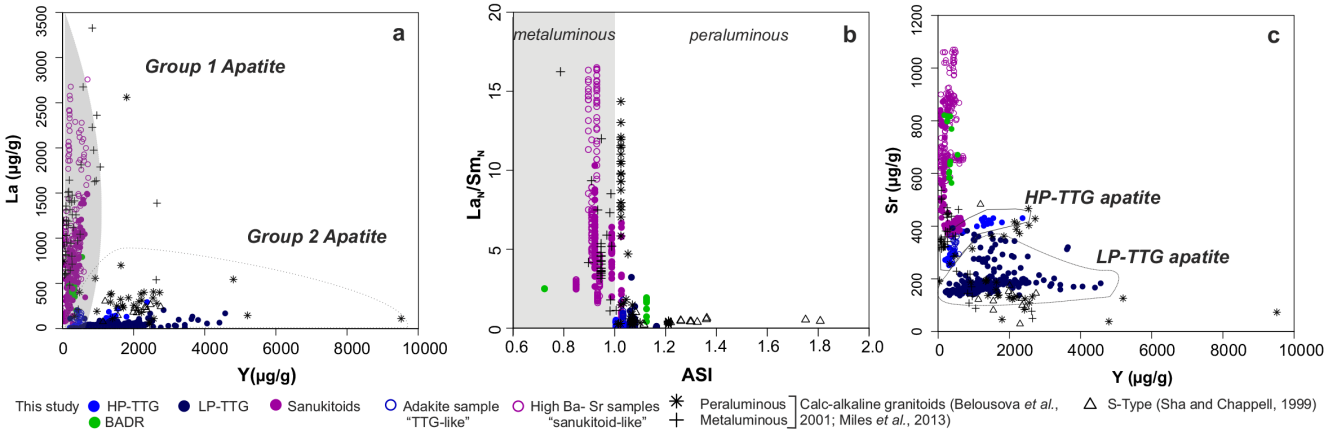

Figure 4 Apatite compositions: **(a)** La *vs.* Y diagram discriminating 2 groups of apatite, **(b)** La_N/Sm_N *vs.* ASI (nAl/((nCa-3.33*nP) + nNa + nK)), discriminating peraluminous from metaluminous compositions and **(c)** Sr *vs.* Y, discriminating apatite from HP- and LP-TTG magmas.

Discussion

The temporal evolution of granitoids has been well established (Fig. 1, see also Moyen and Martin, 2012 for review). Most TTGs can be discriminated on the basis of several whole rock chemical indicators, the most prevalent of which is stronger HREE depletion (Fig. 2j). The present study has also shown systematic differences in TTG apatite and TTG titanite compositions relative to sanukitoids and post-Archean granitoids (Figs. 2, 3), in particular higher Y and HREE contents with low La_N/Sm_N ratio (Figs. 2, 4a). Intriguingly, this is completely opposite to the whole rock signatures (Fig. 2j). In the following text, we attempt to rationalise such observations in terms of possible controls on apatite and titanite chemistry, and in the light of current literature.

Effects of metamorphism and/or deformation. Because Archean rocks may have suffered metamorphism and/or deformation, there is the obvious possibility that accessory mineral chemistry has been modified and records metamorphic/hydrothermal rather than igneous processes. The studies available on the impact of metamorphism and hydrothermalism on apatite and titanite are limited (*e.g.*, Broska *et al.*, 2007) and often describe lithologies and/or whole rock compositions (metapelites or orthogneisses) that are very different from our samples (*e.g.*, Bea and Montero, 1999; Garber *et al.*, 2017). Therefore, in order to test the robustness of apatite and titanite magmatic signatures, we have analysed apatite and titanite from Phanerozoic equivalents of TTG (adakite; Fig. 2b) and sanukitoid (high Ba-Sr granites; Fig. 2e,h), unaffected by any metamorphic event. Their chondrite normalised REE patterns correspond closely to the Archean equivalents (Fig. 2a,d,g) and overlap the relevant fields on the discrimination diagrams above (Figs. 3, 4a).

A few TTG apatite patterns show extreme depletion in LREE with no Eu anomaly (Fig 2a). This can be explained petrographically, by the observed association of secondary allanite and apatite, which form at the expense of primary REE-bearing phases (Fig. S-1). The highly LREE-depleted group in our samples, is therefore interpreted to have formed under high grade metamorphic conditions and are characterised by lower La_N/Sm_N but retains original HREE signatures.

Effects of whole rock composition. The systematic chemical differences between the accessory mineral groups studied here, from different types of granitoid, strongly suggest that bulk rock character exerts strong control on the trace element composition of accessory minerals.

1. The influence of whole rock SiO_2. Partition coefficient studies have shown that incorporation of REE in apatite and titanite increases with SiO_2 of the magma (Prowatke and

Klemme, 2005, 2006). TTGs studied herein vary between 65 wt. % and 74 wt. % SiO_2, the other granitoids range between 53 and 77 wt. %. Within the former, apatite and titanite total REE contents do not systematically increase with [SiO_2] of the melt (Table S-3, Supplementary Information). Furthermore, sanukitoid or BADR samples with similar SiO_{2WR} have apatite and titanite characterised by comparatively higher LREE and lower HREE. Such systematic differences are therefore not controlled simply by silica content.

2. The influence of alumina saturation index (ASI) The striking dichotomy in the TTG between LREE depletion in the accessory minerals and LREE enrichment in whole rocks suggests that another LREE-bearing phase is required for mass balance. Likely contenders would be allanite and monazite, but since these are also common in many other granitoid types, this is unlikely to be the sole explanation.

Figure 4a includes literature data, and highlights the presence of two distinct groups of apatite that are strongly dependent on ASI. ASI < 1 samples (metaluminous) correspond to our sanukitoids-BADR apatites (Group 1), whereas peraluminous samples (ASI > 1) have a comparable chemical signature to TTG apatite grains (low LREE and high HREE-Y, Group 2). This corroborates previous studies on apatite (Harrison and Watson, 1984; Pichavant *et al.,* 1992) and monazite (Montel, 1986) solubilities, which suggest that apatite solubility increases with ASI and (to a lesser extent) with SiO_2 in metaluminous magmas. Conversely, Montel (1986) has shown that monazite solubility decreases as ASI increases. This is also consistent with the presence of "remaining" primary monazite surrounded by secondary allanite and apatite identified on the studied Acasta samples (Supplementary Information). It should be noted that monazite solubity can also be influenced by other factors (*e.g.,* P content in the melt; Skora and Blundy, 2012). In summary, our dataset demonstrates that in peraluminous compositions early monazite will strongly partition LREE with the remaining melt relatively enriched in HREE and Y, which will be incorporated by later apatite and titanite. These conclusions were also reached in previous work on Phanerozoic granitoids (*e.g.,* Chu *et al.,* 2009).

Interestingly, apatites from two metaluminous samples are Y-rich and LREE-poor (Fig. 4a), which is inconsistent with the general trend. These exceptions have the highest SiO_2 content (>73 wt. %), a phenomenon also described by Sha and Chappell (1999). High melt SiO_2 content increases apatite solubility (Harrison and Watson, 1984) and therefore delays its saturation. Consequently, apatite may grow late, allowing early LREE phases (monazite and/or allanite) to incorporate most of the LREE.

3. Other variables. We have shown above that aluminosity and consequent timing of mineral saturation is a first order control on accessory mineral chemistry. However, our TTG apatite compositions have systematically even lower LREE concentrations than published apatite data for peraluminous rocks (Fig. 4a), so other variables must also be important. For example, previous authors have inferred that differences in magmatic apatite composition could be related to magma fO_2 (Sha and Chappell, 1999; Belousova *et al.,* 2001). It remains unclear whether this is linked to the nature of the TTG source (*e.g.,* composition such as high Na_2O and low REE content compared to other granitoids, fO_2, temperature, H_2O-saturated or undersaturated melting) or is another effect of co-crystallising accessory phases. Experimental constraints are currently lacking.

4. The significance of Sr. Previous work (*e.g.,* Halla *et al.,* 2009; Moyen, 2011) has distinguished high pressure TTG, corresponding to a deep source in equilibrium with garnet and rutile but no plagioclase, from low pressure TTG consistent with residual plagioclase. As a direct consequence of residual mineralogy, HP-TTG have low HREE, Nb and Ta and high Sr whereas LP-TTG show the opposite signature for comparable bulk compositions (*e.g.,* Moyen and Martin, 2012). Previous authors (Belousova *et al.,* 2001; Jennings *et al.,* 2011; Bruand *et al.,* 2014) have shown a strong correlation between Sr in apatite and in the corresponding whole rock. Our data sit on this previously reported correlation. Accordingly, in our apatite dataset, two TTG and our adakite samples that have typical HP-TTG signatures have systematically higher Sr concentrations than the others that have LP-TTG signatures (Fig. 4c). Figure 4c also shows that the HP-TTG apatite analyses have lower Y (and by analogy, HREE). All these observations confirm that apatite Sr content can allow discrimination between HP and LP-TTG. Interestingly, correlation between unusually high Sr content of monazite and HP conditions has also been previously reported in the Bohemian Massif peraluminous rocks (Finger and Krenn, 2007).

Implications for crustal evolution research. The preservation of magmatic trace element signatures in apatite and titanite, from metamorphosed terranes such as those of Archean age, provides a useful method to reconstruct ancient magmatic history. For example, in this study, we demonstrate that accessory minerals of late Archean granitoids (sanukitoids) are different from Archean TTGs. Such differences reflect whole rock compositions which themselves reflect petrogenetic processes. Thus, the different petrogeneses of TTGs and sanukitoids (early subduction or "drip tectonics"; Nebel *et al.,* 2018) are reflected by accesssory mineral chemistry. Therefore detailed investigation of the apatite and titanite mineral chemical archive could tightly constrain the change in geodynamics at the end of the Archean. Finally, our data reveal an efficient distinction of parental magma types based on REE-Sr-Y alone which further encourages application to the detrital mineral record. Voluminous data exist from zircons, but the results described above promise much closer constraints on parent rock identity, thus providing vital access to the primary history of eroded terranes and helping to reconstruct the historical evolution of continental crust from the early Earth to the present day.

Acknowledgements

We are grateful to Stuart Kearns and J.-L. Devidal for microanalytical analyses, to Geoff Long for amazing technical support. This work was supported by the Natural Environment Research Council (grant NE/I025573/1) and by the French Government Laboratory of Excellence initiative n° ANR-10-LABX-0006. This is Laboratory of Excellence ClerVolc contribution number 387. We deeply thank the editor H. Marschall and two anonymous reviewers for their input.

Editor: Horst R. Marschall

Additional Information

Supplementary Information accompanies this letter at http://www.geochemicalperspectivesletters.org/article2006.

Cite this letter as: Bruand, E., Fowler, M., Storey, C., Laurent, O., Antoine, C., Guitreau, M., Heilimo, E., Nebel, O. (2020) Accessory mineral constraints on crustal evolution: elemental fingerprints for magma discrimination. *Geochem. Persp. Let.* 13, 7–12.

References

Bea, F., Montero, P. (1999) Behavior of accessory phases and redistribution of Zr, REE, Y, Th, and U during metamorphism and partial melting of metapelites in the lower crust: An example from the Kinzigite Formation of Ivrea-Verbano, NW Italy. *Geochimica et Cosmochimica Acta* 63, 1133-1153.

Belousova, E.A., Walters, S., Griffin, W.L., O'Reilly, S.Y. (2001) Trace-element signatures of apatites in granitoids from the Mt Isa Inlier, Northwestern Queensland. *Australian Journal of Earth Sciences* 48, 603-619.

Broska, I., Harlov, D., Tropper, P., Siman, P. (2007) Formation of magmatic titanite and titanite-ilmenite phase relations during granite alteration in the Tribe?? Mountains, Western Carpathians, Slovakia. *Lithos* 95, 58-71.

Bruand, E., Storey, C., Fowler, M. (2014) Accessory mineral chemistry of high Ba-Sr granites from Northern Scotland: Constraints on petrogenesis and records of whole-rock Signature. *Journal of Petrology* 55, 1619-1651.

Bruand, E., Storey, C., Fowler, M. (2016) An apatite for progress: Inclusions in zircon and titanite constrain petrogenesis and provenance. *Geology* 44, 91-94.

Bruand, E., Fowler, M., Storey, C., Darling, J. (2017) Apatite trace element and isotope applications to petrogenesis and provenance. *American Mineralogist* 102, 75-84.

Bruand, E., Storey, C., Fowler, M., Heilimo, E. (2019) Oxygen isotopes in titanite and apatite, and their potential for crustal evolution research. *Geochimica et Cosmochimica Acta* 255, 144-162.

Chu, M.F., Wang, K.L., Griffin, W.L., Chung, S-L, O'Reilly, S., Pearson, N.J., Iizuka, Y. (2009) Apatite composition: Tracing petrogenetic processes in Transhimalayan granitoids. *Journal of Petrology* 50, 1829-1855.

Finger, F., Krenn, E. (2007) Three metamorphic monazite generations in a high-pressure rock from the Bohemian Massif and the potentially important role of apatite in stimulating polyphase monazite growth along a PT loop. *Lithos* 95, 103-115.

Fowler, M., Rollinson, H. (2012) Phanerozoic sanukitoids from Caledonian Scotland: Implications for Archean subduction. *Geology* 40, 1079-1082.

Garber, J.M., Hacker, B.R., Kylander-Clark, A.R.C., Stearns, M., Seward, G. (2017) Controls on Trace Element Uptake in Metamorphic Titanite : Implications for Petrochronology. *Journal of Petrology* 58, 1031-1058.

Grimes, C.B., Wooden, J.L., Cheadle, M.J., John, B.E. (2015) " Fingerprinting " tectono - magmatic provenance using trace elements in igneous zircon. *Contributions to Mineralology and Petrology* 170, 1-26.

Halla, J., van Hunen, J., Heilimo, E., Höltta, P. (2009) Geochemical and numerical constraints on Neoarchean plate tectonics. *Precambrian Research* 174, 155-162.

Harrison, T.M., Watson, E.B. (1984) The behavior of apatite during crustal anatexis: Equilibrium and kinetic considerations. *Geochimica et Cosmochimica Acta* 48, 1467-1477.

Jennings, E.S., Marschall, H.R., Hawkesworth, C.J., Storey, C.D.; (2011) Characterization of magma from inclusions in zircon: Apatite and biotite work well, feldspar less so. *Geology* 39, 863-866.

Kohn, M.J., Vervoort, J.D. (2008) U-Th-Pb dating of monazite by single-collector ICP-MS: Pitfalls and potential. *Geochemistry, Geophysics, Geosystems* 9, 1-16.

Montel, J.M. (1986) Experimental determination of the solubility of Ce-monazite in SiO2-Al2O3-K2O-Na2O melts at 800°C, 2kbar, under H2O-saturated conditions. *Geology* 14, 659-662.

Moyen, J. (2011) The composite Archaean grey gneisses : Petrological significance, and evidence for a non-unique tectonic setting for Archaean crustal growth. *Lithos* 123, 21-36.

Moyen, J., Laurent, O. (2018) Archaean tectonic systems : A view from igneous rocks. *Lithos* 303, 99-125.

Moyen, J., Martin, H. (2012) Forty years of TTG research. *Lithos* 148, 312-336.

Nasdala, L., Broska, I., Harlov, D.E., Macdonald, R. (2017) Recent progress in the study of accessory minerals. *Mineralogy and Petrology* 102, 431-433.

Nebel, O., Capitanio, F.A., Moyen, J.-F., Weinberg, R.F., Clos, F., Nebel-Jacobsen, Y.J., Cawood, P. (2018) When crust comes of age : on the chemical evolution of Archaean, felsic continental crust by crustal drip tectonics. *Philosophical Transactions of the Royal Society A: Mathematical, Physical and Engineering Sciences* 376, doi: 10.1098/rsta.2018.0103.

Pankhrust, R.J., Weaver, S.D., Bradshaw, J.D., Storey, B.C., Ireland, T.R. (1998) Geochronology and geochemistry of pre-Jurassic superterranes in Marie Byrd Land, Antarctica. *Journal of Geophysical Research* 103, 2529-2547.

Pichavant, M., Montel, J.M., Linda, R. (1992) Apatite solubility in peraluminous liquids : Experimental data and an extension of the Harrison-Watson model. *Geochemica et Cosmochimica Acta* 56, 3855-3861.

Prowatke, S., Klemme, S. (2005) Rare earth element partitioning between titanite and silicate melts: Henry's law revisited. *Geochimica et Cosmochimica Acta* 70, 4997–5012.

Prowatke, S., Klemme, S. (2006) Trace element partitioning between apatite and silicate melts. *Geochimica et Cosmochimica Acta* 70, 4513-4527.

Sha, L.-K., Chappell, B.W. (1999) Apatite chemical composition, determined by electron microprobe and laser-ablation inductively coupled plasma mass spectrometry, as a probe into granite petrogenesis. *Geochimica et Cosmochimica Acta* 63, 3861-3881.

Skora, S., Blundy, J. (2012) Monazite solubility in hydrous silicic melts at high pressure conditions relevant to subduction zone metamorphism. *Earth and Planetary Science Letters* 322, 104-114.

Storey, C.D., Smith, M.P., Jeffries, T.E. (2007) In situ LA-ICP-MS U–Pb dating of metavolcanics of Norrbotten, Sweden: Records of extended geological histories in complex titanite grains. *Chemical Geology* 240, 163-181.

Geochemical Perspectives Letters

Accessory mineral constraints on crustal evolution: elemental fingerprints for magma

E. Bruand, M. Fowler, C. Storey, O. Laurent, C. Antoine, M. Guitreau, E. Heilimo, O. Nebel

Supplementary Information

The Supplementary Information includes:

- Sample Description
- Analytical Techniques
- Tables S-1 to S-3
- Figure S-1
- Supplementary Information References

Sample Description

In this work, we have systematically analysed apatite and titanite (when present) from a range of granitoids from the Archean toward the Phanerozoic (Fig. 1).

TTG and TTG-like

TTG are the main components of Archean cratons and have been interpreted as the results of melted garnet-bearing metabasalt either in subduction or intraplate contexts. They are silica–rich (SiO_2> 64 wt. %), have a high Na_2O content (3-7 wt. %), are low in ferromagnesian, Cr and Ni contents (Moyen and Martin, 2012 and references therein). In this contribution, TTG from different cratons have been studied: Kaapvaal craton (South Africa), Karelia craton (Finland) and the Slave province (Acasta, Canada). In the Kaapvaal craton, the TTG sampled (DWK-04 and HRG-1) are from the Pietersburg block and have been both dated at about 2.9 Ga (Laurent *et al*., 2013). Karelia's samples (EPHE 2004- 369.2 and 413.1) have also been characterised (Mikkola *et al*., 2011) and have been dated at about 2.8 Ga. Acasta samples (AG09-009/14/15 and 16) have previously been characterised for their whole rocks and are dated between 3.9 Ga (AG09-016) and 3.6 Ga (AG09-009/14/15; Guitreau *et al*. 2014; Mojzsis *et al*. 2014). For comparison with those TTG, a TTG-like sample was also analysed. It is an early Permian biotite microgranite from Marie Byrd Land (Antarctica). This sample exposes the same whole rock characteristics as the TTG (high SiO_2, sodic nature, low K_2O/Na_2O <0.5, High Sr >400 and La, low Y; Pankhrust *et al*., 1998) and is therefore belonging to the high-silica adakites group previously defined by Martin *et al*. (2005). Their main petrographic characteristics are compiled in Table S.1. All samples have apatite and zircon as accessory phases. One sample has titanite (EPHE 2004- 369.2) and sample AG09 009 has small grains of primary monazite surrounded by secondary allanite, apatite and grains of thorite (Antoine *et al*., personal communication). All Acasta's samples have clusters of secondary fibrous allanite.

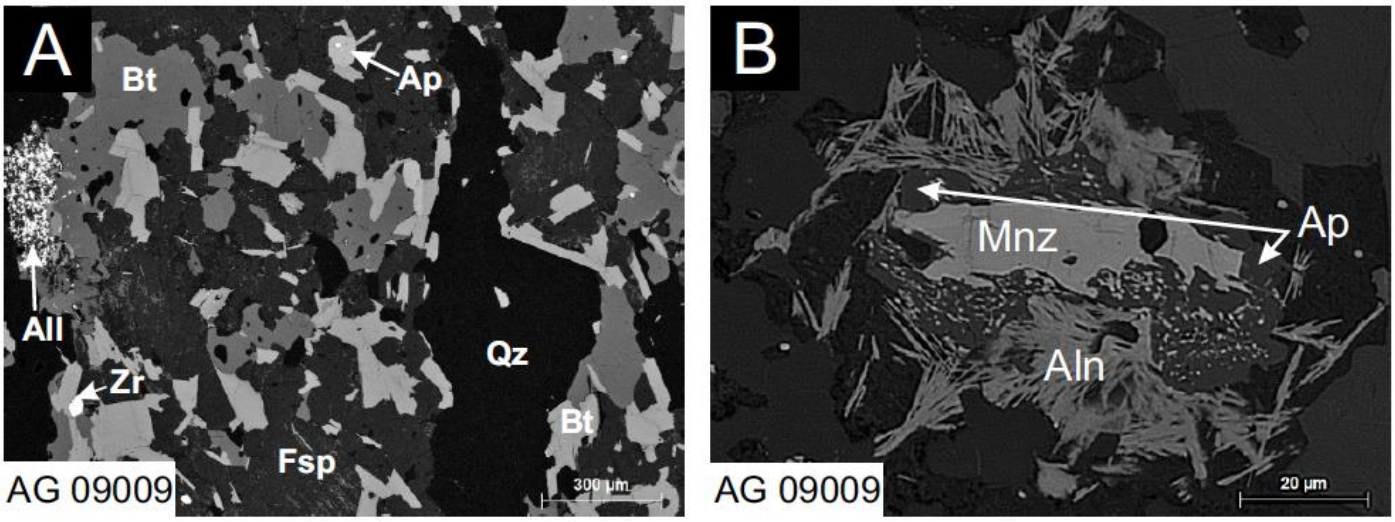

Figure S-1 BSE images of TTG (Acasta) with aggregates of secondary fibrous allanite. Careful study of the samples allowed to find preserved primary monazite partly replaced by secondary allanite, apatite and thorite due to later metamorphic overprinting (Antoine *et al*., personal communication).

Sanukitoids and High Ba-Sr granite

Sanukitoids are typical magmas appearing at the Archean-Proterozoic transition. Their chemistries have been interpreted as the result of the interaction between a melt or fluid and a mantle wedge. They are chemically characterised by silica contents up to 60 wt. %, Cr > 100 ppm, high Na_2O, K_2O, Sr, Ba and LREE contents (Martin *et al*., 2005).

Sanukitoids samples in this study are from the Karelia and Kaapvaal cratons. Sanukitoids from Kaapvaal are a granodiorite and a diorite from the Limpopo belt (MAT 43 and MAT 13, Laurent *et* al., 2014a,b, 2017; Laurent and Zeh, 2015) and have been dated around 2.7 Ga. Karelia's samples have also been dated around 2.7 Ga (Heilimo *et al*., 2011) and are both granodioritic in composition.

The high Ba-Sr suite studied here are the modern equivalent of the sanukitoids (Fowler and Rollinson, 2012). They are Caledonian granitoids that have been characterised for major, trace, Nd ans O isotopes whole rock composition (Fowler *et al*., 2001; Fowler *et al*., 2008). The whole-rock chemistry of the selected samples range from granodiorite to granitic compositions. They are located in the northwestern part of Scotland and have been dated at about 425 Ma (Kocks *et al*., 2014). Description of their mineralogy can be found in Bruand *et al*. (2014). All samples contain apatite, titanite and zircon with some containing allanite or monazite. Trace elements data on accessory phases available in this contribution are from Bruand *et al*. (2014).

Basalt-Andesite-Dacite-Rhyolite (BADR)

The "modern" granitoids samples (BADR samples) studied in this contribution are from the Guernsey igneous complex (Channel Island) which is part of the Armorican massif and is divided geologically into two main parts. The southern part mainly comprises Paleoproterozoic gneisses (The Icartian gneisses; Samson *et al*., 2003) intruded by syntectonic and subsequently deformed Neoproterozoic granitoids (Perelle quartz-diorite and l'Erée granite; Samson and D'Lemos 1999) and the northern part is dominated by the undeformed, Neoproterozoic Northern Igneous Complex. In order to cover the entire Neoproterozoic plutonic history, samples studied here are from deformed (11-EG-07) and undeformed granitoids (11-BD-02). Sample 11-BD-02 is a diorite while 11-EG-07 is a granodiorite (Table S-1). Plutonic rocks from the Northern Igneous Complex have a calc-alkaline signature and were emplaced at the end of the Cadomian orogeny (*ca*. 560-550 Ma, de Bremond d'Ars *et al*., 1992). They are referred to by Brown *et al*. (1990) as post-tectonic units. The deformed sample from l'Erée granite (EG-07) in the southern part of the island and its field relationships (e.g. the presence of dykes absent in the north and the presence of foliation) indicate that it belongs to the early Cadomian event and intruded the Icartian basement syntectonically. This is also suggested by age data (Samson et *al*., 2003) at 614 Ma +/- 2 Ma. The early Cadomian intrusions in the Channel Islands are calc-alkaline in composition and have typical volcanic arc granites signature (Power *et al*., 1990). Accessory phases found in the Guernsey igneous complex are apatite, zircon and +/- titanite.

Table S-1 Sample description.

(a)

		Type	Age (Ma)	literature	Comments	Accessories
Kaapvaal craton, South Africa	DWK-04	TTG	2941	Laurent *et al.*, 2013; Laurent *et al*, 2014a,b WR	Trondhjemite	apatite, zircon
	HRG-1	TTG	2933		Trondhjemite	apatite zircon
	MAT 13	Sanukitoid	2679	Laurent *et al.*, 2013; Laurent *et al.*, 2014a,b WR	Granodiorite	apatite, titanite, zircon
Karelia craton, Finland	EPHE 2004 369.2	TTG	2821	Mikkola *et al.*, 2011 corresponding sample A1857	Granodiorite	apatite, titanite, zircon, aln
	EPHE 2013 413.1	TTG	2785	Käpyaho *et al.*, 2006 corresponding sample A1705	Tonalite	apatite, zircon
	STHA-2009-316	Sanukitoid	2722	Heilimo *et al.*, 2011 corresponding sampleA1339	Granodiorite	apatite, titanite, zircon
	A572	Sanukitoid	2723	Heilimo *et al.*, 2011	Granodiorite	apatite, titanite, zircon
Marie Byrd Land, Antartica	402-1D	Adakite	early permian	Pankhrust *et al.*, 1998	Biotite microgranite	apatite, zircon
High Ba-Sr, Scotland	SR1	Sanukitoid-like	425	Fowler *et al.*, 2008; Fowler and Rollinson, 2012	Granodiorite	apatite, titanite, zircon
	SR2	Sanukitoid-like	425		Appinite	apatite, titanite, zircon
	SR3	Sanukitoid-like	425		Granodiorite	apatite, titanite, zircon, aln
	SR4	Sanukitoid-like	425		Granodiorite	apatite, titanite, zircon
	RA1	Sanukitoid-like	425	Kocks *et al.*, 2014; Fowler *et al.*, 2001, 2008; Fowler and Rollinson, 2012	Appinite	apatite, titanite, zircon
	RT1	Sanukitoid-like	425		Tonalite	apatite, titanite, zircon, aln
	R2	Sanukitoid-like	425		Tonalite	apatite, titanite, zircon, aln
	RGH1	Sanukitoid-like	425		Granite	apatite, titanite, zircon
Slave Province, Acasta, Canada	AG09 009	TTG	3600	Mojzsis *et al.*, 2014 for WR and Guitreau *et al.*, 2012 for dating	Granitic orthogneiss	apatite, zircon, monazite
	AG09 014	TTG	3600		Tonalitic orthogneiss	apatite, zircon
	AG09 015	TTG	3600		Tonalitic orthogneiss	apatite, zircon
	AG09 016	TTG	3947		Tonalitic orthogneiss	apatite, zircon
Guernsey Igneous Province, Channel Islands	11-BD-02	Arc Magma-Diorite	560-550	Unpublished data in Samson *et al.*, (2003)	Bordeaux diorite locality	apatite, titanite, zircon
	11-EG-07	Arc Magma - Granite	614		L'Erée granite locality/granodiorite	apatite, titanite, zircon

(b)

Sample	GPS Coordinates	Sample	GPS Coordinates	Sample	GPS Coordinates
DWK-04[1]	Lat 23.611944S Long 30.328889E	AG09016[3]	Lat 65.160650N Long 115.546033W	SR4[6]	Lat 56.730766N Long 5.540805W
HRG-1[1]	Lat 23.792512S Long 29.127496E	402.1D[4]	Lat 75.00S Long 112.53W	SR3[6]	Lat 56.685100N Long 5.627994W
EPHE 2004 369.2[2]	Lat 65.27511096N Long 29.18714509E	STHA-2009-316[5]	Lat 63.22764732N Long 30.65472253E	SR1[6]	Lat 56.689443N Long 5.602272W

EPHE 2013-413.1[2]	Lat 64.1841557N Long 28.874444 E	A572[5]	Lat 64.44985108N Long 29.00994815E	RT1[6]	Lat 57.993611N Long 4.197395W
AG09009[3]	Lat 65.170217N Long 115.562683W	MAT-13[1]	Lat 23.525368S Long 29.703366E	11-EG-07[7]	Lat 49.454750N Long 2.655250W
AG09014[3]	Lat 65.160250N Long 115.547317W	RHG-1[6]	Lat 58.010645N Long 4.250916W	11-BD-02[7]	Lat 49.490000N Long 2.578361W
AG09015[3]	Lat 65.160250N Long 115.547317W	R2[6]	Lat 57.996508N Long 4.185728W		

[1]Kaapvaal craton, Laurent *et al.* (2014a,b); [2]Karelia craton, Mikkola *et al.* (2011) and Käpyaho *et al.* (2006); [3]Slaves, craton, Mojzsis *et al.* (2006); [4]Byrd Land granitoid, Pankhrust *et al.* (1998); [5]Karelia craton, Heilimo *et al.* (2011); [6]High Ba-Sr, Fowler *et al.* (2008, 2011); [7] Guernsey samples.

Analytical Techniques

The samples were crushed (jaw-crusher, ball mill or Selfrag™), sieved (<355 μm, 355-500 μm and 500-1000 μm fractions) and passed over a Wilfley table. A diamagnetic separator was then used to obtain fractions of different heavy minerals based on their diamagnetic properties. Titanite and apatite were handpicked, mounted in epoxy resin discs and polished for in-situ chemical analysis. Titanite and apatite have also been analysed within thick sections (c. 150 μm).

Image acquisition

Back-scattered electron (BSE) images of titanite were taken with a scanning electron microscope (SEM) JEOL JSM-6100 at the University of Portsmouth (accelerating voltage = 20 kV). Cathodoluminescence (CL) images of apatite were taken with a KeDev Centaurus cathodoluminescence detector housed within a JEOL 6060LV SEM at the University of Portsmouth, or a JEOL JSM-5910 LV with an OPEA detector at the Laboratoire Magmas et Volcans (Clermont-Ferrand, France; accelerating voltage = 15 kV).

Electron probe microanalysis (EPMA)

A Cameca SX-100 microprobe at Bristol University was used for determination of major elements in titanite and zircon using TAP, LPET, PET and LLIF crystals. PC0, TAP, LPET and LLIF crystals were used for apatite. An electron beam of 1 μm was used for titanite and 10 μm for apatite, both with 20 kV accelerating voltage and, 40nA and 10 nA beam currents respectively. An electron beam of 5 μm was used for zircon with an accelerating voltage of 17 kV and a beam current of 100 nA. Several trace elements in these minerals were also analysed for comparison with laser ablation ICP-MS (LA-ICPMS) data. The Durango apatite standard (Marks *et al.*, 2012) and the 91500 zircon standard (Wiedenbeck *et al.*, 2004) were analysed during sessions to monitor data quality.

Trace element analysis : LA-ICPMS

Trace element contents of titanite and apatite were determined by LA-ICPMS at the University of Portsmouth using an Agilent 7500cs (quadrupole) ICPMS and a New-Wave UP213 (λ=213 nm) solid state Nd:YAG laser, or at the Laboratoire Magmas et Volcans (Clermont-Ferrand, France) using an Element XR associated with an excimer laser ATL (Resonetics M-50E; λ = 193 nm). Each analysis consisted of *ca.* 30 s background acquisition and 60 to 80 s sample acquisition. The diameter of the laser beam was 30 μm for titanite and 9-30 μm for apatite.

Internal references used for normalisation of LA-ICPMS data were ^{43}Ca for apatite and titanite and were obtained by EPMA. Details of instruments conditions can be found in Table S-2. Geochemical Data Toolkit (GCDkit, Version 5.0; Janousek *et al.* 2006) was used to plot the data. **All data trace elements on accessory phases and whole rock data presented in this contribution can be found in Table S-3, available for download as an Excel file from http://www.geochemicalperspectivesletters.org/article2006.**

Table S-2 Laser models and conditions to measure apatite and titanite trace elements.

	Frequence	Fluence	Laser Spot	External Standard	Secondary standard analysed during runs
Excimer laser ATL 193 nm Resonetics M-50E with XR Element (Laboratoire Magmas et Volcans)	1-2 Hz	2.8-2.9 J/cm²	9-12 µm	NIST 610 (Pearce *et al.*, 1997) or GSE-1G (Jochum *et al*, 2005)	Durango for Apatite (Marks *et al*., 2013)
New-Wave UP213 (l=213 nm) solid state Nd:YAG laser and 7500 cs Agilent (University of Portsmouth)	10 Hz	4 J/cm²	30 µm	NIST 610	Durango for Apatite (Marks *et al*., 2013) and in house Khan standard for titanite
Excimer laser S155 Resonetics with Element 2 (Goethe Universitaet Frankfurt)	5 Hz	3-4 J/cm²	29 µm	NIST 610	Durango

Table S-3 Whole rock analysis and trace elements analysis on apatite and titanite from the different samples studied in this contribution. Chondrite values used for normalisation are from Boynton (1984).

Table S-3 can be downloaded as an Excel file from http://www;geochemicalperspectivesletters.org/article2006.

Supplementary Information References

Boynton, W.V. (1984) Chapter 3 - Cosmochemistry of the Rare Earth Elements: Meteorite Studies. In: Henderson P (ed) *Rare Earth Element Geochemistry*. Elsevier, 63–114

Brown, M., Power, G.M., Topley, C.G., D'Lemos, R.S. (1990) Cadomian magmatism in the North Armorican Massif. *Geological Society of London*, Spec Publ 51,181–213. doi: 10.1144/GSL.SP.1990.051.01.12;

Bruand, E., Storey, C., Fowler, M. (2014) Accessory mineral chemistry of high Ba-Sr granites from Northern Scotland: Constraints on petrogenesis and records of whole-rock Signature. *Journal of Petrology 55*, 1619-1651. doi: 10.1093/petrology/egu037.

De Bremond d'Ars, J., Martin, H., Auvray, B., Lécuyer, C. (1992) Petrology of a magma chamber: the Plutonic Complex of Guernsey (Channel Islands, UK). *Journal of the Geological Society of London* 149, 701–708. doi: 10.1144/gsjgs.150.4.0788;

Fowler, M., Rollinson, H. (2012) Phanerozoic sanukitoids from Caledonian Scotland: Implications for Archean subduction. *Geology* 40, 1079–1082. doi: 10.1130/G33371.1

Fowler, M., Henney, P.J., Darbyshire, D.P.F., Greenwood, P.B. (2001) Petrogenesis of high Ba-Sr granites: the Rogart pluton, Sutherland. *Journal of the Geological Society of London* 158, 521–534. doi: 10.1144/jgs.158.3.521.

Fowler, M., Kocks, H., Darbyshire, D.P.F., Greenwood, P.B. (2008) Petrogenesis of high Ba-Sr plutons from the Northern Highlands Terrane of the British Caledonian Province. *Lithos* 105, 129–148. doi: 10.1016/j.lithos.2008.03.003.

Guitreau, M., Blichert-Toft, J., Martin, H., Mojzsis, S.J., Albarède, F. (2012) Hafnium isotope evidence from Archean granitic rocks for deep-mantle origin of continental crust. *Earth and Planetary Science Letters* 337, 211-223.

Guitreau, M., Blichert-Toft, J., Mojzsis, S.J., Roth, A.S.G., Bourdon, B., Cates, N.L., Bleeker, W. (2014) Lu-Hf isotope systematics of the Hadean-Eoarchean Acasta Gneiss Complex (Northwest Territories, Canada). *Geochimica et Cosmochimica Acta* 135, 251–269. doi: 10.1016/j.gca.2014.03.039.

Heilimo, E., Halla, J., Huhma, H. (2011) Single-grain zircon U-Pb age constraints of the western and eastern sanukitoid zones in the Finnish part of the Karelian Province. *Lithos* 121, 87–99. doi: 10.1016/j.lithos.2010.10.006.

Janousek, V., Farrow, C.M., Erban, V. (2006) Interpretation of Whole-rock Geochemical Data in Igneous Geochemistry : Introducing Geochemical Data Toolkit (GCDkit). *Journal of Petrology* 47, 1255–1259. doi: 10.1093/petrology/egl013;

Jochum, K.P., Willbold, M., Raczek, I., Stoll, B., Herwig, K. (2005). Chemical Characterisation of the USGS Reference Glasses GSA-1G, GSC-1G, GSD-1G, GSE-1G, BCR-2G, BHVO-2G and BIR-1G Using EPMA, ID-TIMS, ID-ICP-MS and LA-ICP-MS. *Geostandards and Geoanalytical Research* 29, 285-302.

Käpyaho, A., Mänttäri, I., Huhma, H. (2006) Growth of Archaean crust in the Kuhmodistrict. Eastern Finland: U–Pb and Sm–Nd isotope constraints on plutonic rocks. *Precambrian Research* 146, 95–119.

Kocks, H., Strachan, R., Evans, J., Fowler, M. (2014) Contrasting magma emplacement mechanisms within the Rogart igneous complex, NW Scotland, record the switch from regional contraction to strike-slip during the Caledonian orogeny. *Geological Magazine* 151, 899–915.

Laurent, O., Paquette, J-L, Martin, H., Doucelance, R. (2013) LA-ICP-MS dating of zircons from Meso- and Neoarchean granitoids of the Pietersburg block (South Africa): Crustal evolution at the northern margin of the Kaapvaal craton. *Precambrian Research* 230, 209–226. doi: 10.1016/j.precamres.2013.02.009.

Laurent, O., Martin, H., Moyen, J.F., Doucelance, R. (2014a) The diversity and evolution of late-Archean granitoids: Evidence for the onset of "modern-style" plate

tectonics between 3.0 and 2.5 Ga. *Lithos* 205, 208–235. doi: 10.1016/j.lithos.2014.06.012.

Laurent, O., Rapopo, M., Stevens, G., Moyen, J-F, Martin, H., Doucelance, R., Bosq, C. (2014b) Contrasting petrogenesis of Mg–K and Fe–K granitoids and implications for post-collisional magmatism: Case study from the Late-Archean Matok pluton (Pietersburg block, South Africa). *Lithos* 196–197, 131–149. doi: 10.1016/j.lithos.2014.03.006

Laurent, O., Zeh, A. (2015) A linear Hf isotope-age array despite different granitoid sources and complex Archean geodynamics : Example from the Pietersburg block (South Africa). *Earth and Planetary Science Letters* 430, 326–338. doi: 10.1016/j.epsl.2015.08.028.

Laurent, O., Zeh, A., Gerdes, A., Villaros, A. (2017) How do granitoid magmas mix with each other ? Insights from textures , trace element and Sr – Nd isotopic composition of apatite and titanite from the Matok pluton (South Africa). *Contributions to mineralogy and Petrology* 172, 80 doi: 10.1007/s00410-017-1398-1

Marks, M.A., Wenzel, T., Whitehouse, M.J., Loose, M., Zack, T., Barth, M., Worgard, L., Krasz, V., Eby, G.N., Stosnach, H. (2012) The volatile inventory (F, Cl, Br, S, C) of magmatic apatite: An integrated analytical approach. *Chemical Geology* 291, 241-255.

Martin, H., Smithies, R.H., Rapp, R., Moyen, J-F, Champion, D. (2005) An overview of adakite, tonalite-trondhjemiten-granodiorite (TTG), and sanukitoid: Relationships and some implications for crustal evolution. *Lithos* 79, 1–24. doi: 10.1016/j.lithos.2004.04.048.

Mikkola, P., Huhma, H., Heilimo, E., Whitehouse, M. (2011) Archean crustal evolution of the Suomussalmi district as part of the Kianta Complex, Karelia: Constraints from geochemistry and isotopes of granitoids. *Lithos* 125, 287–307. doi: 10.1016/j.lithos.2011.02.012.

Mojzsis, S.J., Cates, N.L., Caro, G., Trail, D., Abramov, D., Guitreau, M., Blichert-Toft, J., Hopkins, M.D., Bleeker, W. (2014) Component geochronology in the polyphase ca. 3920Ma Acasta Gneiss. *Geochimica Cosmochimica Acta* 133, 68–96. doi: 10.1016/j.gca.2014.02.019.

Moyen, J-F, Martin, H. (2012) Lithos Forty years of TTG research. *Lithos* 148, 312–336. doi: 10.1016/j.lithos.2012.06.010.

Pankhrust, R.J., Weaver, S.D., Bradshaw, J.D., Storey, B.C., Ireland, T.R. (1998) Geochronology and geochemistry of pre-Jurassic superterranes in Marie Byrd Land, Antartica. *Journal of Geophysical Research* 103, 2529–2547.

Pearce, N.J., Perkins, W.T., Westgate, J.A., Gorton, M.P., Jackson, S.E., Neal, C.R., Chenery, S.P. (1997) A compilation of new and published major and trace element data for NIST SRM 610 and NIST SRM 612 glass reference materials. *Geostandards and Geoanalytical Research* 21, 115-144.

Power, G.M., Brewer, T.S., Brown, M., Gibbons, W. (1990) Late Precambrian foliated plutonic complexes of the Channel Islands and La Hague: early Cadomian plutonism. *Geological Society of London*, Spec Publ 51, 215–229. doi: 10.1144/GSL.SP.1990.051.01.13

Samson, S.D., D'Lemos, R.S. (1999) A precise late Neoproterozoic U-Pb zircon age for the syntectonic Perelle quartz diorite, Guernsey, Channel Islands, UK. *Geological Society of London* 156, 47–54. doi: 10.1144/gsjgs.156.1.0047

Samson, S.D., D'Lemos, R.S., Blichert-Toft, J., Vervoort, J. (2003) U-Pb geochronology and Hf-Nd isotope compositions of the oldest Neoproterozoic crust within the Cadomian orogen: New evidence for a unique juvenile terrane. *Earth and Planetary Science Letters* 208, 165–180. doi: 10.1016/S0012-821X(03)00045-1